

## Accepted Manuscript

Highly efficient removal of Cr(VI) from water with nanoparticulated zerovalent iron: understanding the Fe(III)-Cr(III) passive outer layer structure

V. Nahuel Montesinos, Natalia Quici, E. Beatriz Halac, Ana G. Leyva, Graciela Custo, Silvina Bengio, Guillermo Zampieri, Marta I. Litter

PII: S1385-8947(14)00118-1  
DOI: <http://dx.doi.org/10.1016/j.cej.2014.01.093>  
Reference: CEJ 11735

To appear in: *Chemical Engineering Journal*

Received Date: 3 September 2013  
Revised Date: 26 January 2014  
Accepted Date: 29 January 2014

Please cite this article as: V. Nahuel Montesinos, N. Quici, E. Beatriz Halac, A.G. Leyva, G. Custo, S. Bengio, G. Zampieri, M.I. Litter, Highly efficient removal of Cr(VI) from water with nanoparticulated zerovalent iron: understanding the Fe(III)-Cr(III) passive outer layer structure, *Chemical Engineering Journal* (2014), doi: <http://dx.doi.org/10.1016/j.cej.2014.01.093>

This is a PDF file of an unedited manuscript that has been accepted for publication. As a service to our customers we are providing this early version of the manuscript. The manuscript will undergo copyediting, typesetting, and review of the resulting proof before it is published in its final form. Please note that during the production process errors may be discovered which could affect the content, and all legal disclaimers that apply to the journal pertain.



1                   **Highly efficient removal of Cr(VI) from water with**  
2                   **nanoparticulated zerovalent iron: understanding the Fe(III)-**  
3                   **Cr(III) passive outer layer structure**

4  
5                   V. Nahuel Montesinos<sup>a,b,c</sup>, Natalia Quici<sup>a,b</sup>, E. Beatriz Halac<sup>d</sup>, Ana G. Leyva<sup>c,e</sup>, Graciela  
6                   Custo<sup>a</sup>, Silvina Bengio<sup>f</sup>, Guillermo Zampieri<sup>b,g</sup>, Marta I. Litter<sup>a,b,d,h,\*</sup>

7  
8                   <sup>a</sup> *Gerencia Química, Comisión Nacional de Energía Atómica, Av. Gral. Paz 1499, 1650 San*  
9                   *Martín, Prov. de Buenos Aires, Argentina*

10                   <sup>b</sup> *Consejo Nacional de Investigaciones Científicas y Técnicas, Av. Rivadavia 1917, 1033*  
11                   *Ciudad Autónoma de Buenos Aires, Argentina*

12                   <sup>c</sup> *Departamento de Química Inorgánica, Analítica y Química Física, FCEN, Universidad de*  
13                   *Buenos Aires, Ciudad Universitaria Pabellón II, 1428 Ciudad Autónoma de Buenos Aires,*  
14                   *Argentina*

15                   <sup>d</sup> *Gerencia de Investigación y Aplicaciones, Comisión Nacional de Energía Atómica, Av.*  
16                   *Gral. Paz 1499, 1650 San Martín, Prov. de Buenos Aires, Argentina*

17                   <sup>e</sup> *Escuela de Ciencia y Tecnología, Universidad de Gral. San Martín, Campus Miguelete,*  
18                   *Martín de Irigoyen 3100, 1650 San Martín, Prov. de Buenos Aires, Argentina*

---

\* Corresponding author. Tel: +54 011 6772 7942  
e-mail address: [litter@cnea.gov.ar](mailto:litter@cnea.gov.ar), [marta.litter@gmail.com](mailto:marta.litter@gmail.com)

1 <sup>f</sup> *Instituto Balseiro, Universidad Nacional de Cuyo, Av. Bustillo 9500, 8400 Bariloche, Prov.*  
2 *de Río Negro, Argentina*

3 <sup>g</sup> *Centro Atómico Bariloche, Comisión Nacional de Energía Atómica, Av. Bustillo 9500, 8400*  
4 *Bariloche, Prov. de Río Negro, Argentina*

5 <sup>h</sup> *Instituto de Investigación e Ingeniería Ambiental, Universidad Nacional de Gral. San*  
6 *Martín, Peatonal Belgrano 3563, 1° piso (1650), San Martín, Prov. de Buenos Aires,*  
7 *Argentina*

8

9 **Abstract**

10 Nanoscale zerovalent iron (nZVI) particles were successfully employed for Cr(VI)  
11 removal from aqueous solutions at pH 3. It was found that the capacity of the system  
12 increases with increasing nZVI dosage. Starting at 300  $\mu\text{M}$ , a complete Cr(VI) conversion  
13 was achieved in 30 min with a Fe:Cr(VI) molar ratio (*MR*) of 3, and 45% conversion with *MR*  
14 = 1 over the same period of time. The material exhibited an enhanced reactivity in comparison  
15 with other previously tested similar materials.

16 The proposed mechanism involves an initial reduction of Cr(VI) to Cr(III) by reaction  
17 with  $\text{Fe}^0$  or Fe(II) on the particle surface or in solution (secondary pathway), followed by an  
18 arrest on Cr(VI) removal attributed to the passivation of the surface of the nanoparticles.  
19 Passivation was confirmed by Raman and X-ray photoelectron spectroscopic (XPS).  
20 Furthermore, XPS analysis demonstrated that Cr(III) is the only Cr species present in the  
21 external layer of the nanoparticles after the reaction. Raman analysis and XPS measurements

1 performed after mild sputtering showed that nZVI exposed to Cr(VI) presented a structure,  
2 from outside to inside, of hydroxchromites  $\rightarrow$  magnetite  $\rightarrow$  Fe<sup>0</sup>.

3

4 *Keywords:* Hexavalent chromium, nanoscale zerovalent iron, XPS analysis, Raman  
5 spectroscopy

ACCEPTED MANUSCRIPT

## 1    **1.    Introduction**

2

3            Hexavalent chromium is the Cr species that presents the highest environmental threat  
4 in aqueous systems, due to its toxicity to biological organisms, high solubility and mobility.  
5 The toxicological effects of Cr(VI) originate on its oxidative nature in water, as well as on the  
6 formation of free radicals during the reduction of Cr(VI) to Cr(III) occurring inside the cell  
7 [1]. Consequently, the World Health Organization [2] recommends a 0.05 mg L<sup>-1</sup> maximum  
8 contaminant level of Cr(VI) in drinking water, while total chromium should be discharged  
9 below 2 mg L<sup>-1</sup> according to US EPA regulations [3].

10            In the last two decades, it has been demonstrated that zerovalent iron (ZVI) materials  
11 are a good alternative for the removal of a wide range of pollutants including metals and  
12 metalloids in water, showing a high efficiency and low economic and environmental costs [4-  
13 9]. More recently, the use of ZVI nanoparticles (nZVI), proved to be a promising and more  
14 efficient version of this technology [10-17]. In addition to showing an enhanced reactivity,  
15 their larger surface area and higher penetrability in soil make these particles also a very  
16 powerful tool for on-site treatment. In particular, Cr(VI) sequestration with ZVI [18-22] and  
17 nZVI [23-29] has been extensively studied. The general process can be described as the  
18 reduction of Cr(VI) to Cr(III) coupled with the oxidation of Fe<sup>0</sup> to Fe(II) and Fe(III), and the  
19 subsequent precipitation of sparingly soluble iron hydroxochromites [4].

20            Due to its reductive nature and to the fact that the corrosion of the material is  
21 thermodynamically favoured in the presence of oxygen, ZVI particles unavoidably develop a  
22 thin film of oxides on the surface, being extensively accepted that this external film has a

1 fundamental role on Cr(VI) sequestration. The protective layer of iron oxides continuously  
2 grows at the Fe<sup>0</sup>/oxide layer interface while being simultaneously destroyed by dissolution or  
3 restructuring at the oxide layer/H<sub>2</sub>O interface. A porous structure, which can be considered  
4 multi-layered, with increasing density from the external oxide layer to the metallic core, is  
5 created [30]. The passive film is generally described by a two-layer model constituted by  
6 magnetite (Fe<sub>3</sub>O<sub>4</sub>) and maghemite (γ-Fe<sub>2</sub>O<sub>3</sub>) [31, 32]. The variable arrangement of the oxides  
7 forming the shell has been described by several models, e.g.: a) an inner layer of Fe<sub>3</sub>O<sub>4</sub> and a  
8 γ-Fe<sub>2</sub>O<sub>3</sub> outer layer at the oxide-solution interface, b) less discrete layers constituted by  
9 amorphous oxides, or c) a layer of mixed oxides with a Fe(II) concentration gradient  
10 decreasing from Fe<sub>3</sub>O<sub>4</sub> to γ-Fe<sub>2</sub>O<sub>3</sub> towards the surface [31, 32]. The electron transfer from the  
11 Fe<sup>0</sup> core to the contaminants depends strongly on the composition of this layer, which can act  
12 as a semiconductor or coordinating surface [32] and affects the mass transport [30]. Fe<sup>0</sup> can  
13 be regarded as a long-term source of highly reactive hydroxides or oxides [33].

14 In this work, Cr(VI) removal in aqueous solution was analyzed by using very reactive  
15 commercial nZVI particles at different Fe:Cr(VI) molar ratios (*MR*). The effect of the *MR*  
16 used in the Cr(VI) removal was evaluated and a possible mechanism was postulated.

17

18

19

20

21

22

## 1    2.    **Materials and methods**

2

### 3    2.1.    *Chemicals*

4

5            Cr(VI) solutions were prepared using  $K_2Cr_2O_7$  provided by Mallinckrodt. nZVI  
6 (NANOFER 25, hereafter N25) was provided by NANO IRON, s.r.o. (Czech Republic) as a  
7 suspension in water and kept at low temperature ( $\sim 4\text{ }^\circ\text{C}$ ) until used. *o*-phenantroline  
8 (Mallinckrodt),  $H_2SO_4$  (Biopack), ascorbic acid (Carlo Erba), 1,5-diphenylcarbazide (UCB),  
9 phosphoric acid (Biopack) were of analytical reagent grade and used without further  
10 purification. In all experiments, Milli-Q water was used (resistivity =  $18\text{ M}\Omega\text{ cm}$ ).

11

### 12    2.2.    *Experimental setup*

13

14            Batch experiments were carried out in a 400 mL cylindrical jacketted Pyrex glass  
15 reactor. Temperature was controlled by recirculating water through the jacket using a  
16 Polyscience 9106 Circulator, and the content was stirred by a vertical paddle agitator  
17 (Decalab). The experimental setup is shown in Fig. S1 of the Supplementary Data (SD).

18            Preliminary experiments were performed at pH 3, 5 and 7 and, from them, pH 3 was  
19 chosen as the working pH for most experiments. All experiments were carried out with 200  
20 mL of  $300\text{ }\mu\text{M}$  Cr(VI) solution, previously adjusted at pH 3 with  $0.2\text{ M}$   $H_2SO_4$  and open to  
21 the atmosphere. Cr(VI) solutions were stirred for 15 min to achieve oxygen saturation before  
22 each experiment ( $7.2 - 7.6\text{ mg L}^{-1}$ ), and no change in  $[O_2]$  took place during Cr(VI) removal

1 with N25. Finally, nZVI particles were added to the system in the 150 - 900  $\mu\text{M}$  range  
2 (expressed as total Fe), corresponding to a Fe:Cr(VI) *MR* range of 0.5 - 3. A few additional  
3 experiments were carried out at pH 5, keeping all other conditions equal, with nZVI in the  
4 300 - 3000  $\mu\text{M}$  range.

### 5 6 2.3. *Analytical methods*

7  
8 In all experiments, 4 mL samples were periodically withdrawn and separated in four 1  
9 mL aliquots, which were centrifuged in Eppendorf tubes during 2 min using an Eppendorf  
10 MiniSpin® centrifuge at 13000 rpm. The supernatant of each sample was used separately for  
11 Cr(VI), Fe(II), Fe<sub>total</sub> and Cr<sub>total</sub> analysis. [Cr(VI)] was measured spectrophotometrically using  
12 the diphenylcarbazide method at 540 nm [34]. [Fe(II)] and [Fe<sub>total</sub>] were measured  
13 spectrophotometrically using the *o*-phenanthroline method at 508 nm [35]. UV-vis absorption  
14 measurements were performed employing a UV-visT80+ spectrophotometer (PG instrument  
15 Ltd). [Cr<sub>total</sub>] was measured employing Total Reflection X-ray Fluorescence (TXRF) [36]  
16 using a solution of [Co(II)] = 10  $\mu\text{M}$  as internal standard. A total reflection system comprising  
17 an X-ray spectrometer, an X-ray tube excitation system, a total reflection module and  
18 spectrum acquisition and quantitation software was used. The X-ray spectrometer consisted of  
19 an 80 mm Si(Li) detector with 166 eV of full width half maximum (FWHM) for 5.9 keV, a  
20 0.008 mm thick Be window, an Ortec 672 fast spectroscopy amplifier and an analog-to-digital  
21 converter (ADC) Nucleus PCA2. Excitation conditions were 50 kV and 30 mA in all cases  
22 and the spectrum acquisition time was 300 s in every case. Initial and final pH determinations



1 were carried out using a pH-meter (Meterlab PH M210), and dissolved O<sub>2</sub> was measured with  
2 an oxygen sensor (Hach Sens Ion 156 Multiparameter Meter) equipped with a Hach DO meter  
3 electrode. As shown in reference [29] temperature is a determinant parameter in Cr(VI)  
4 removal by nZVI, therefore all experiments were performed at  $24 \pm 1$  °C at least by duplicate,  
5 and the results averaged. The experimental error was calculated as the standard deviation of  
6 replicate experiments and was never higher than 10%.

7

#### 8 2.4. *nZVI characterization*

9

10 X-ray diffraction (XRD), Raman spectroscopy and XPS analysis were carried out to  
11 characterize nZVI particles before and after exposure to Cr(VI). After the treatment, the solid  
12 particles were filtered using 0.22 µm cellulose acetate membranes (Osmoionics), washed  
13 three times with 2 mL Milli-Q water and preserved under vacuum for 24 h before the analysis.  
14 XRD patterns were obtained with a Philips PW-3710 X-ray diffractometer, using Cu Kα  
15 radiation. Data for Raman spectroscopic measurements were acquired in a LabRAM HR  
16 Raman system (Horiba JobinYvon), equipped with a confocal microscope, two  
17 monochromator gratings and a charge coupled device detector (CCD). An 1800 g/mm grating  
18 and 100 µm hole results in a 2 cm<sup>-1</sup> spectral resolution. The 514.5 nm line of an Ar<sup>+</sup> laser was  
19 used as the excitation source. Measurements were carried out in a backscattering geometry,  
20 with an objective magnification of 50×. Acquisition time was 180 s and 4 accumulations. XPS  
21 spectra were taken with a hemispherical electrostatic energy analyzer ( $r = 10$  cm) using Al  
22 Kα radiation ( $h\nu = 1486.6$  eV). Mild sputtering experiments were performed with an Ar beam

1 of 2 keV ion energy and a current density of around  $10 \mu\text{A cm}^{-2}$ ; in these conditions, a  
2 sputtering rate of a few  $\text{\AA min}^{-1}$  is expected. Scanning electron microscopy (SEM) analysis  
3 was performed with a Q200 FEI Company equipment only for N25 samples. In this case,  
4 suspended nanoparticles were seeded in a copper-aluminium support and dried under vacuum  
5 24 h before the analysis. The supported sample was coated with a thin gold film to improve its  
6 conductivity and, therefore, the resolution of SEM images.

7

### 8 **3. Results and discussion**

#### 9 *3.1. N25 characterization*

10

11 The nanoparticles present a core-shell like structure with a  $\text{Fe}^0$ -rich core surrounded by  
12 a magnetite-rich shell. The most important characteristics of the N25 particles, are presented  
13 in Table S1 (SD). Fig. S2(a) (SD) shows the X-ray diffraction pattern of the commercial  
14 nanoparticles, where two distinct phases can be distinguished: one corresponding to  $\alpha$ -Fe, and  
15 the second one assigned either to magnetite and/or to maghemite. Those two phases cannot be  
16 differentiated by the technique under our experimental conditions. However, this ambiguity  
17 was resolved by Raman spectroscopy, displayed in Fig. S2(b), which indicates that the only  
18 iron oxide phase present in the initial nZVI sample is magnetite. The mean crystallite size was  
19 estimated from the FWHM of the  $\alpha$ -Fe peak located at  $45^\circ$ , using the Scherrer equation. The  
20 obtained value was approximately 70 nm, in close agreement with the results provided by the  
21 manufacturer. The SEM image of fresh N25 particles is shown in Fig. S3 (SD). It can be

1 observed that the freshly seeded material is disposed as irregular agglomerates with a fine  
2 structure composed of spherical nanoparticles with an estimated diameter of 65 nm.

3 The characterization analysis confirmed all data provided by the supplier.

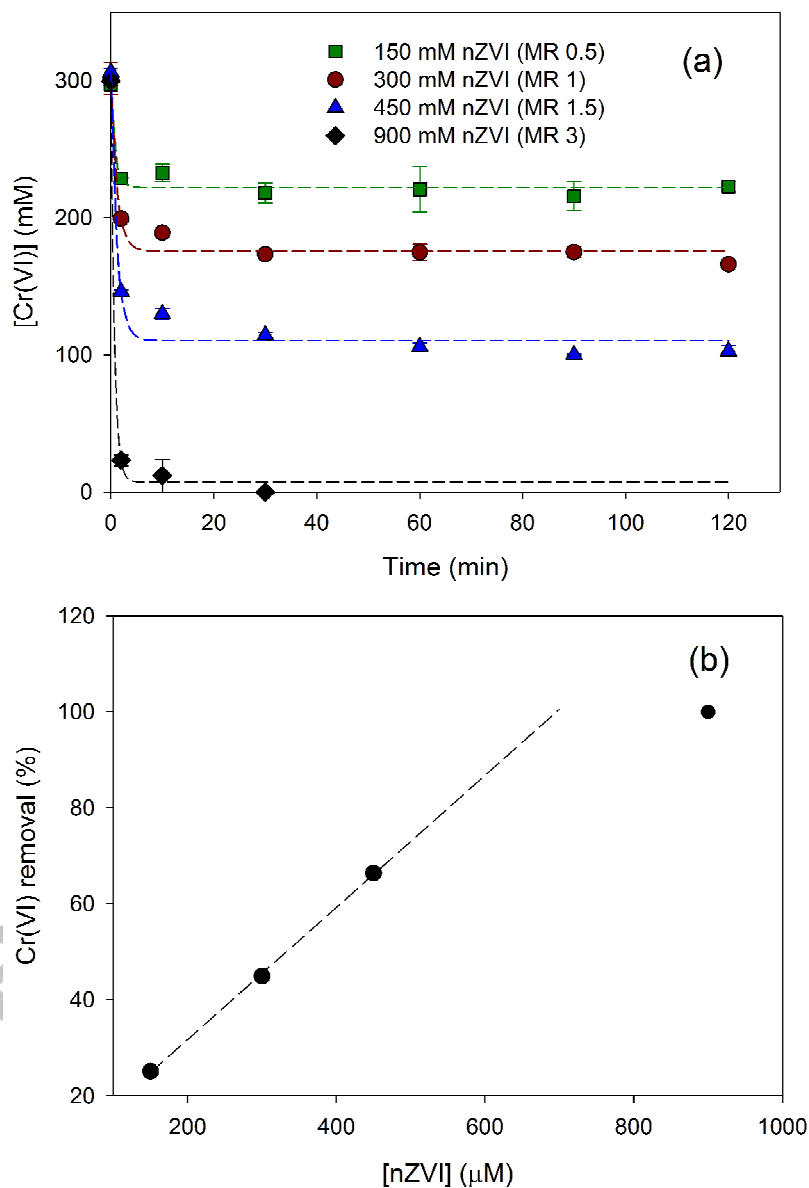
### 4 5 3.2. *Experiments of Cr(VI) removal*

6  
7 Results of the experiments aimed at evaluating the performance of N25 particles on  
8 Cr(VI) removal at pH 3 are displayed in Fig. 1. This working pH was selected after a series of  
9 preliminary experiments at pH 3, 5 and 7, because this condition showed the highest reactivity  
10 and allowed a good inspection of the temporal concentration profiles. At higher pH values,  
11 removal efficiency was much lower.

12 As it can be observed in Fig. 1(a), removal of dissolved Cr(VI) increased with the  
13 initial nZVI mass, with complete removal with  $[nZVI] = 900 \mu M$  (*MR 3*) after 30 min. A very  
14 rapid initial Cr(VI) conversion during the first 10 minutes was followed by a plateau in all  
15 cases. Therefore, the maximum Cr(VI) removal was reached in only 10 min. As the best  
16 (complete) conversion was found for *MR 3* at 30 min, the percentage of Cr(VI) removed after  
17 that time for all *MR* was plotted against the amount of nZVI. Fig. 1(b) indicates a linear  
18 behaviour, with the exception of *MR 3*, where the nZVI particles seem to still preserve Cr(VI)  
19 removal power.

20

21



1

2 Fig. 1. (a) [Cr(VI)] vs. time for removal experiments with different *MR*; (b) percentage of  
 3 Cr(VI) removal after 30 min of treatment vs. [nZVI]. Conditions: [Cr(VI)] = 300 μM, pH 3, *T*  
 4 = 24 ± 1 °C. Dashed curves are only for better visualization of points and do not correspond  
 5 to a fitting model.

1           The performance obtained in this work is the highest registered for Cr(VI) removal  
 2 with nZVI to our knowledge, in comparison with previous works. Table 1 lists the Cr(VI)  
 3 removal efficiency of different nanoparticulated materials in terms of mg of Cr(VI) removed  
 4 per gram of nZVI, taken from the literature [24, 25, 27].

5

6       Table 1

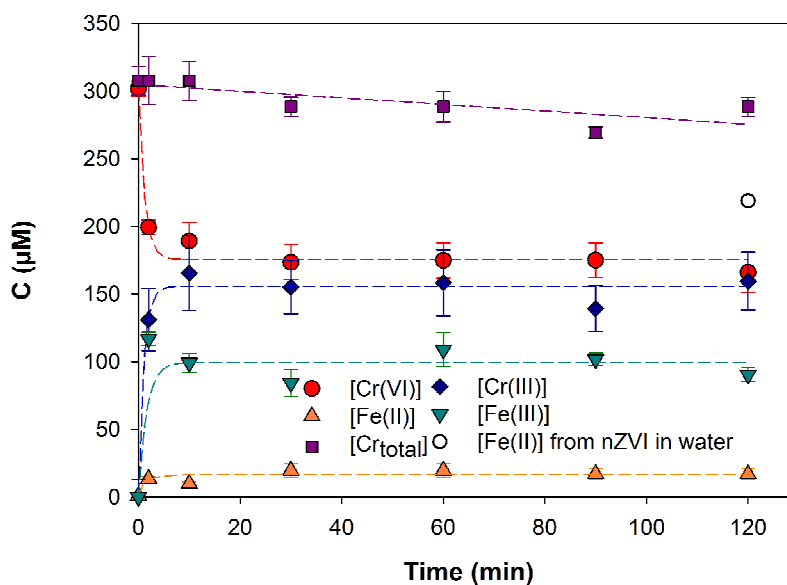
7       Mass of Cr(VI) removed per gram of nZVI for different nZVI materials.

mg Cr(VI)/g nZVI	pH	Reference
10.06	6.36	Ai et al. 2008 [25]
50 - 180	4 - 8	Li et al. 2008 [24]
34.1	6	Kim et al. 2012 [28]
62.4	6	Wang et al.2011 [26]
20.16	5	Alidokht et al. 2011 [27]
180	4.82	Fang et al. 2011 [37]
100	3	Lv et al. 2012 [38]
47.2 ± 0.1	5	This work
411 ± 24	3	This work

8

9

10           In order to achieve a better understanding of the system, concentrations of Fe(II),  
 11 Fe(III) and  $Cr_{total}$  were measured during the time span of the reaction. *MR* 1 was chosen to  
 12 allow a proper inspection of the experimental data; results are displayed in Fig. 2.



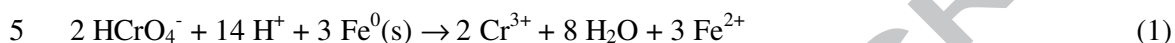
1

2 Fig. 2. Time profiles of [Cr(VI)], [Cr(III)], [Fe(II)], [Fe(III)] and [Cr<sub>total</sub>] for Cr(VI) treatment  
 3 with nZVI. Conditions: [Cr(VI)] = 300 μM, [nZVI] = 300 μM (MR 1), pH 3,  $T = 24 \pm 1$  °C.  
 4 [Fe(II)] from [nZVI] = 300 μM in water after 120 min at pH 3 and  $T = 24 \pm 1$  °C is also  
 5 plotted as an open circle. Dashed curves are only for better visualization of points and do not  
 6 correspond to a fitting model.

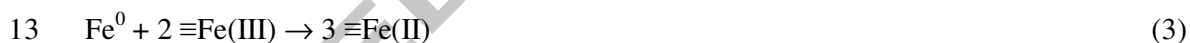
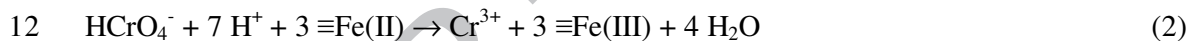
7

8 Fig. 2 shows that around 50% of Cr(VI) is removed after 120 min, leaving Cr(III) in  
 9 solution and 94% of total chromium still dissolved, indicating that direct Cr(VI) adsorption  
 10 does not take place under our experimental conditions or at least it could not be perceived due  
 11 to fast reduction on the surface. Additionally, it can be observed that Cr(VI) removal is  
 12 coupled with a partial dissolution of the nanoparticles introducing iron in the aqueous phase;  
 13 both processes, removal and dissolution stop simultaneously after 10 minutes.

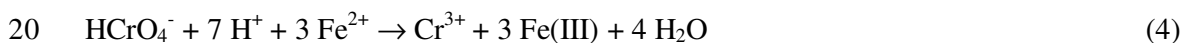
1           The main proposed pathway for Cr(VI) removal by ZVI materials [22] comprises the  
 2 heterogeneous Cr(VI) reduction involving direct electron transfer from Fe<sup>0</sup> ( $E_{\text{Fe}^{2+}/\text{Fe}^0}^0 = -0.44$   
 3 V) to Cr(VI) ( $E_{\text{HCrO}_4^-/\text{Cr}^{3+}}^0 = 1.36$  V):



6  
 7           As postulated in ref. [39], Cr(VI) can be reduced by Fe(II) at the surface (indicated as  
 8  $\equiv\text{Fe}(\text{II})$ , equation (2)), as Fe(II) in the solid is a more reducing species than Fe(II) in solution  
 9 (indicated as Fe<sup>2+</sup>) [40]. Further regeneration of  $\equiv\text{Fe}(\text{II})$  can occur after the surface reaction  
 10 between Fe<sup>0</sup> with  $\equiv\text{Fe}(\text{III})$  (equation (3)):



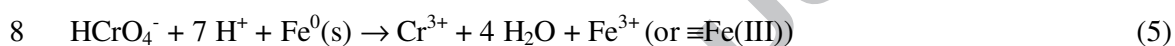
13  
 14  
 15           On the other hand, a minor pathway that cannot be fully ruled out at pH 3 [38]  
 16 involves the homogenous Cr(VI) reduction by dissolved Fe<sup>2+</sup> ions (equation **Error!**  
 17 **Reference source not found.** (4)), having the same stoichiometry than equation (2) but  
 18 with less reducing power [40].



20  
 21

1           Only 11% of the initial Cr(VI) could be removed through this minor pathway  
2 (equation (4)), as it can be calculated by mass balance and using the concentrations of  
3 iron species from Fig. 2. Fang et al. [37] measured the extent of this pathway by capturing  
4 dissolved  $\text{Fe}^{2+}$ , and found a reduction in Cr(VI) removal efficiency of 7.4%, in good  
5 agreement with the 11% estimated in this work. Thus, the overall reaction for Cr(VI)  
6 reduction by nZVI is represented by equation (5):

7



9

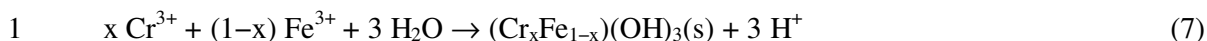
10 Consistently with equation (5), in all experiments, a slight increase in pH ( $\approx \Delta\text{pH} = 0.4$ ) was  
11 observed.

12           Even though it is not possible to determine the exact extent of Cr(VI) reduction by  
13  $\text{Fe}^{2+}$  compared with the reduction at the surface of the nanoparticles (equations (1) and (2)),  
14 the fact that iron dissolution and Cr(VI) removal stopped simultaneously at 30 min (Fig. 2)  
15 evidences a connection between these two processes. The arrest in Cr(VI) removal together  
16 with the interrupted iron dissolution would indicate the poisoning of the nZVI surface. This is  
17 in accordance with the precipitation of Cr(III) at the surface as amorphous  $\text{Cr}(\text{OH})_3$  [18, 41]  
18 or Fe(III)-Cr(III) hydr(oxydes) that has been previously associated with the passivation of the  
19 surface of iron nanoparticles [24]. The formation of the solid compounds is represented by  
20 equations (6)-(8):

21







3 The surface passivation hypothesis was supported by the fact that the amount of Fe(II)  
4 found in solution after 120 min of stirring nZVI (300  $\mu\text{M}$ ) in water in the absence of Cr(VI)  
5 (Fig. 2)  $[\text{Fe}^{2+}]$  was higher than in the same experiment with Cr(VI) (219 against 16  $\mu\text{M}$ ,  
6 respectively).

7 It is worth mentioning that direct corrosion of the nZVI particles by  $\text{O}_2$  is not likely to  
8 be extensively developed under the present experimental conditions since their oxidation by  
9 Cr(VI) is thermodynamically and kinetically favoured ( $E^0_{\text{HCrO}_4^-/\text{Cr}^{3+}}$  is 1.36 V, i.e., more  
10 positive than that of  $\text{O}_2/\text{H}_2\text{O}$  (1.23 V)). In agreement, as said in the Experimental Section,  
11 preliminary experiments showed that no changes in the concentration of oxygen took place  
12 during Cr(VI) removal with N25.

13 As a final refinement of the process, the product of the reaction, Cr(III), could be  
14 removed in a subsequent step by alkalization. As known, Cr(III) toxicity and mobility is  
15 lower than that of Cr(VI) and, hence, the removal process is able to reduce the toxicity of the  
16 initial solution. Fe(II) and Fe(III), which are non-toxic, remain in solution as 0.94 and 5.04  
17  $\text{mg L}^{-1}$ , respectively (Fig. 2) and would be precipitated also by the alkalization step.

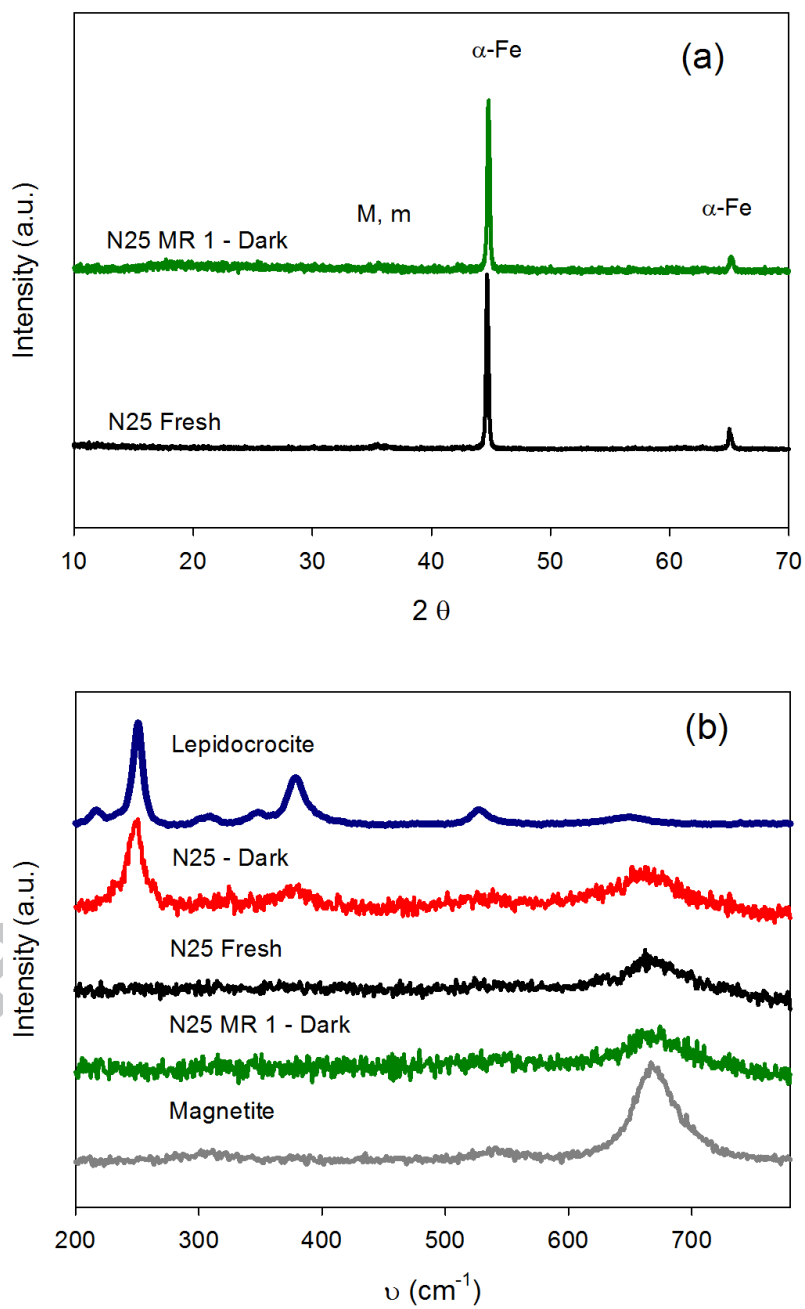
18

19 3.3. *XRD and Raman analysis of the solids*

20

21 Fig. 3(a) compares the XRD pattern of the initial N25 particles sample with that of the  
22 solid obtained after 120 min of contact with Cr(VI) (MR 1). It can be seen that, after Cr(VI)

1 treatment, no evidence of new iron phases is observed. Fig. 3(b) shows the Raman spectra of  
2 fresh N25 particles, the solid after 120 min of Cr(VI) treatment at *MR* 1 (N25 MR 1), and the  
3 solid obtained after 120 min when N25 was in contact with water in the absence of Cr(VI)  
4 (N25 W). Spectra of pure lepidocrocite and magnetite samples are also shown. When nZVI  
5 was in contact with Cr(VI), the only iron oxide phase present after 120 min was magnetite, as  
6 in the original material. However, in the absence of Cr(VI), lepidocrocite was detected in  
7 addition to the magnetite phase. Lepidocrocite is an Fe(III) oxyhydroxide commonly formed  
8 as an electrochemical corrosion product of iron in acid media in excess of dissolved O<sub>2</sub> (> 3  
9 mg L<sup>-1</sup>) [42], conditions existing actually in our system, as indicated in the experimental  
10 section. The fact that lepidocrocite is not formed in the presence of Cr(VI) strongly suggests  
11 that Cr(VI) reduction at the surface of nZVI particles prevents further changes in the outer  
12 layer. In this way, neither Cr(VI) reduction nor corrosion can further occur.



1

2 Fig. 3. (a) X-ray diffraction patterns of nZVI particles before (N25 Fresh) and after 120  
3 minutes of Cr(VI) treatment with MR 1 (N25 MR 1). Magnetite (M), maghemite (m) and  $\alpha$ -

1 Fe reference peaks are indicated; (b) Raman spectra of fresh N25 particles (N25 Fresh), nZVI  
2 after 120 min in contact with Cr(VI) at *MR* 1 (N25 MR 1), and after 120 min in water in the  
3 absence of Cr(VI) (N25 W). Conditions: pH 3,  $T = 24 \pm 1$  °C. Raman spectra of pure  
4 lepidocrocite and magnetite samples are also displayed.

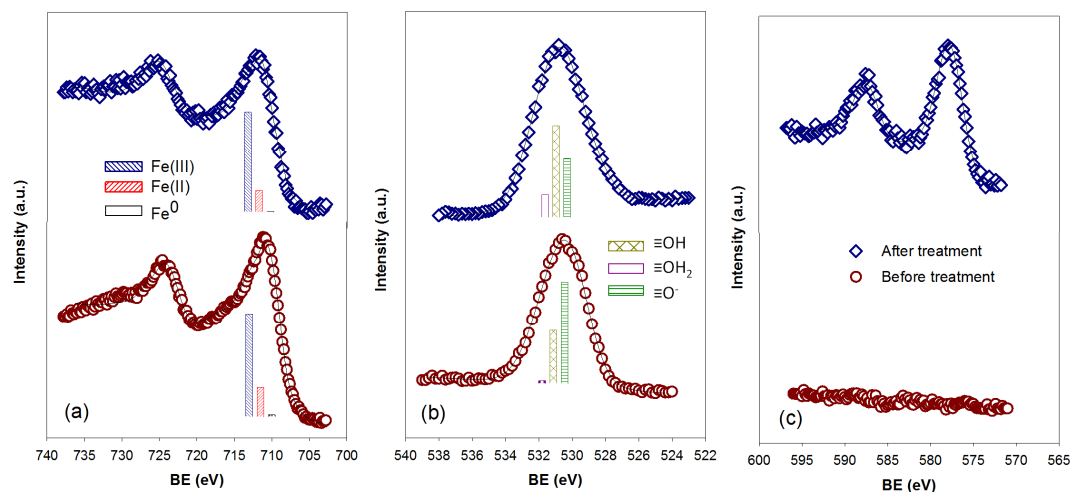
5

### 6 3.4. XPS analysis of nZVI before and after Cr(VI) removal experiments

7

8 Fig. 4 shows the XPS spectra taken for samples of N25 before treatment (N25 Fresh)  
9 and after treatment of a Cr(VI) solution with *MR* 1. Both samples present the spin-orbit split  
10 Fe 2p peaks at around 711 and 724 eV with signals composed of photoelectrons from Fe<sup>0</sup>,  
11 Fe(II) and Fe(III) (Fig. 4(a)) and a broad O 1s peak at 531 eV with contributions of ≡O<sup>-</sup>, ≡OH  
12 and ≡OH<sub>2</sub> components (Fig. 4(b)). The peak fitting methodology description is provided in  
13 the SD, especially indicated for the case of the Fe 2p spectra in Fig. S4. After 120 min  
14 treatment with 300 μM Cr(VI), two new peaks appeared at 577 and 586 eV, corresponding to  
15 the Cr 2p<sub>3/2</sub>-2p<sub>1/2</sub> photoelectrons (Fig. 4(c)). The binding energies (BE) and the spin-orbit  
16 splitting of the Cr 2p peaks are in good agreement with those reported for Cr<sub>2</sub>O<sub>3</sub> or Cr(OH)<sub>3</sub>  
17 [43]. This indicates that Cr(III) is the only species present at the surface, in agreement with  
18 the fact that Cr(VI) adsorption does not take place or, if it takes place, Cr(VI) is  
19 instantaneously reduced on the surface. A detailed analysis shows that the maximum of the Fe  
20 2p<sub>3/2</sub> peak shifts from 710.8 eV in the fresh material to 711.5 eV after the Cr(VI) treatment  
21 (Fig. 4(a)), consistent with oxide and hydroxide environments, respectively. The analysis of  
22 the O 1s peaks (Fig. 4(b)) supports this concept by showing an increase in the proportion of

1  $\equiv\text{OH}$  and  $\equiv\text{OH}_2$  over  $\equiv\text{O}^-$  components after the treatment. Being the mean free path for iron  
 2 equivalent to 6 atomic layers, in the case of a monolayer of Cr(III) adsorbed on the surface of  
 3 the nZVI particles, an approximate ratio of Cr:Fe intensities = 1:5 would have been expected  
 4 as the mean free path and the photoemission cross section of Fe 2p and Cr 2p are similar [43].  
 5 However in the *MR* 1 sample, the analysis of the Cr:Fe intensity ratio indicates a 1:1 value  
 6 which denotes that Cr(III) is incorporated into the solid structure.



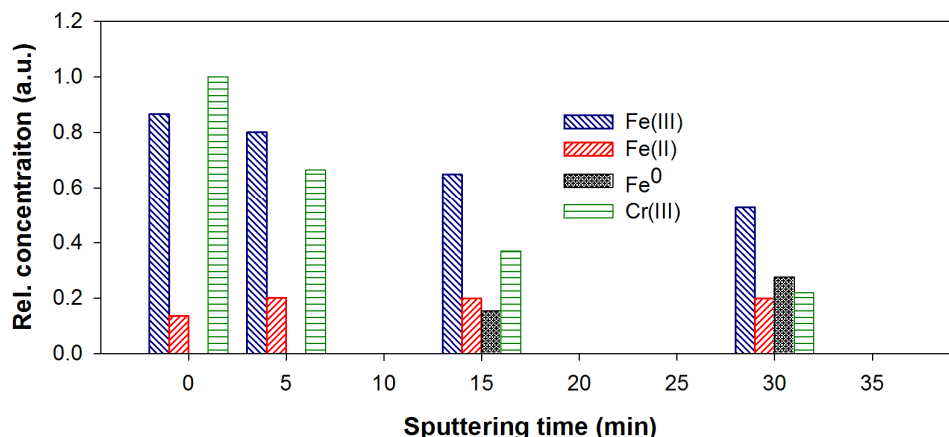
7  
 8 Fig. 4. XPS spectra of fresh N25 particles and after 120 minutes of Cr(VI) treatment with *MR*  
 9 1. (a) Fe 2p (b) O 1s peaks (c) Cr 2p and for the solids obtained before (lower curve) and after  
 10 120 min in contact with Cr(VI) (upper curve). Conditions:  $[\text{Cr(VI)}] = 300 \mu\text{M}$ , pH 3,  $T = 24 \pm$   
 11  $1^\circ\text{C}$ . The intensity scale (a.u.) is the same for Fe 2p, O 1s and Cr 2p peaks.

13 Formation of alloy-like passivating Cr-Fe hydroxides on the surface of nZVI has been  
 14 reported previously [6, 23, 24]. Manning et al. [23] studied the solid product obtained after  
 15 Cr(VI) treatment with nZVI by EXAFS, XANES and XPS, finding that only Cr(III) is

1 retained in the surface as a poorly ordered  $\text{Cr}(\text{OH})_3$  and/or a mixed phase of  $\text{Cr}_x\text{Fe}_{1-x}(\text{OH})_3$ . Li  
2 et al. [24] analyzed the chromium deposition on the nZVI surface using high-resolution X-ray  
3 photoelectron spectroscopy (HR-XPS), finding the stoichiometry of the chromites to be  
4 approximately Cr/Fe 2:1, i.e.  $(\text{Cr}_{0.67}\text{-Fe}_{0.33})(\text{OH})_3$  or  $\text{Cr}_{0.67}\text{Fe}_{0.33}\text{OOH}$ . According to the  
5 authors, after reaching the oxide surface of the nanoparticles, Cr(VI) would be initially  
6 reduced to  $\text{Cr}(\text{OH})_3$  and then incorporated to the FeOOH structure in the form of chromites.

7 In order to analyze the nZVI particles composition as a function of depth from the  
8 surface before and after Cr(VI) treatment, mild sputtering experiments were performed; XPS  
9 spectra of N25 Fresh and *MR* 1 samples were taken over time. Fig. 5 shows the relative  
10 concentration of  $\text{Fe}^0$ , Fe(II), Fe(III) and Cr(III) in the exposed surface over sputtering time for  
11 the *MR* 1 sample. The relative concentration of the iron phases was calculated as  $[\text{Fe } 2\text{p}]_i / [\text{Fe } 2\text{p}]_T$ ,  
12 where  $[\text{Fe } 2\text{p}]_i$  is the total area of the peak of the *i*th iron component and  $[\text{Fe } 2\text{p}]_T$  the  
13 total Fe 2p signal for each sample. For Cr(III), the relative concentration was calculated as  $[\text{Cr } 2\text{p}]_t / [\text{Cr } 2\text{p}]_0$ ,  
14 where  $[\text{Cr } 2\text{p}]_t$  is the area of the Cr 2p peak at time “t” and  $[\text{Cr } 2\text{p}]_0$  the area of  
15 the Cr 2p peak at time “0”. A clear increase in the  $\text{Fe}^0$  signal is observed, and it proves that  
16 the sputtering is removing the external iron oxide shell from the nanoparticles. As said before  
17 [27, 28] several models have been used to describe the iron oxide film from a two-layer  
18 discrete model to a gradient of mixed oxides. In our case, a more complete description of the  
19 layer can be obtained after the XPS results because an increase in the Fe(II):Fe(III) ratio  
20 indicates that the structure of the oxide film is a Fe(II)-Fe(III) iron oxide with a continuous  
21 Fe(II) gradient towards the interior of the nanoparticles, consistent with the detection of a  
22 magnetite phase by Raman spectroscopy.

1



2

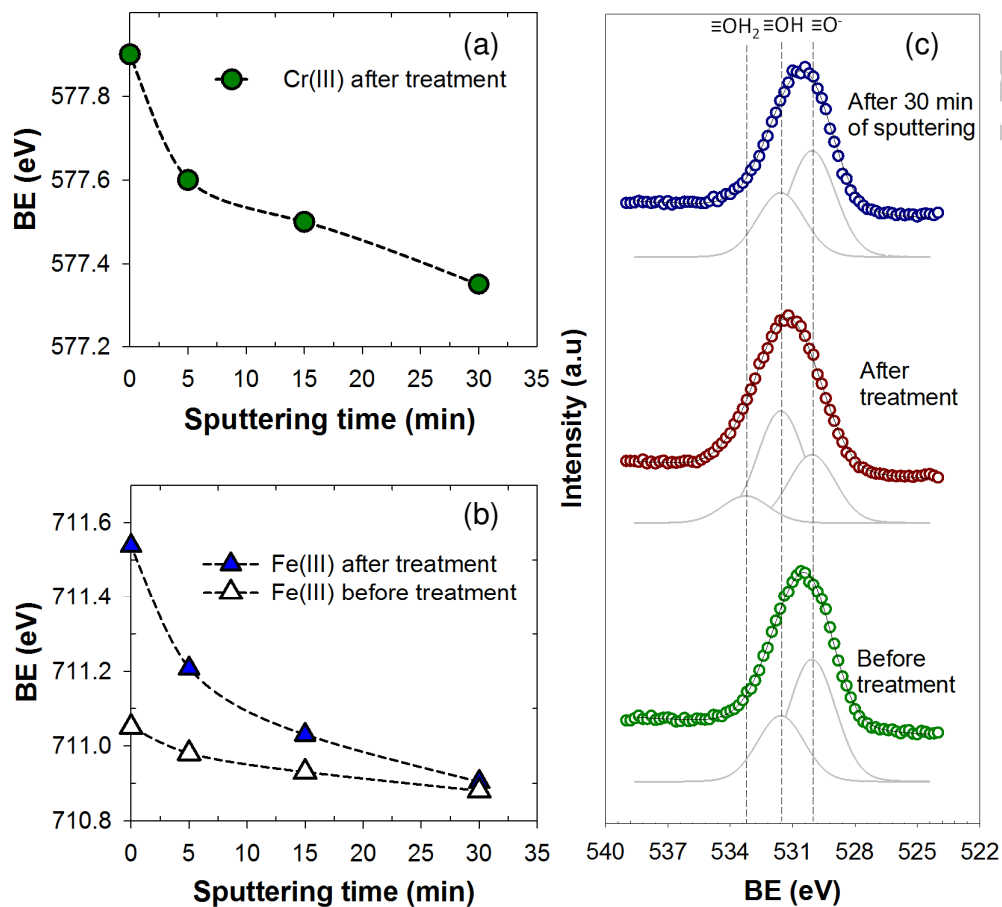
3 Fig. 5. Time evolution of relative concentrations of Fe<sup>0</sup>, Fe(II), Fe(III) and Cr(III) in N25 MR

4 1.

5 On the other hand, a clear decrease in Cr(III) concentration is observed as long as the  
 6 oxide film is removed by sputtering, revealing that Cr is trapped only in the surface of the  
 7 nZVI, leaving a still reactive Fe<sup>0</sup> enriched core that cannot be exploited for Cr(VI) removal,  
 8 due to the formation of a Cr(III)-Fe(III) passive film.

9 As revealed by Fig. 6(a) and 6(b), as long as the sputtering removes layers from the  
 10 nZVI after treatment, a clear decrease in the BE of Cr(III) and Fe(III) is observed. This  
 11 behaviour corresponds to the transition from a more hydroxy/oxyhydroxy environment to a  
 12 pure oxide phase and is consistent with the composition of oxygenated species displayed in  
 13 Fig. 6(c). The intensity of oxygen forming  $\equiv\text{OH}$  and  $\equiv\text{OH}_2$  increases after the treatment and  
 14 decreases after 30 minutes of sputtering, where the  $\equiv\text{O}^-$  component is dominant. This is not  
 15 the case of N25 Fresh, where, as shown in Fig. 6, the BE hardly changes with sputtering time  
 16 and the environment is constituted only by  $\equiv\text{O}^-$ .

1



2

3 Fig. 6. BE shifts over sputtering time for (a) Cr(III) and (b) Fe(III) peaks, centred around  
 4 577.5 and 710.5 eV, before and after treatment of a Cr(VI) solution in a MR 1; and (c) O 1s  
 5 XPS spectra before and after treatment and after 30 min of sputtering. Conditions as in Fig. 5.

6

7 As indicated before, Li et al. [21] calculated the stoichiometry of Cr(III) incorporated  
 8 to the FeOOH structure as  $(\text{Cr}_{0.67}\text{-Fe}_{0.33})(\text{OH})_3$  or  $\text{Cr}_{0.67}\text{Fe}_{0.33}\text{OOH}$ . However, this  
 9 stoichiometry relies on the assumption of a constant Cr:Fe ratio for the nanoparticles after



1 treatment. In contrast, our XPS and Raman analyses of the nZVI exposed to Cr(VI) suggest a  
2 structure, from outside to inside, of hydroxchromites  $\rightarrow$  magnetite  $\rightarrow$  Fe<sup>0</sup> and, thus, a  
3 decreasing Fe(III) and Cr(III) concentration gradient seems to be a more accurate model.

#### 4 5 **4. Conclusions**

6  
7 nZVI has been proven to be an efficient Cr(VI) removal agent that, combined with an  
8 alkaline precipitation step, should adjust chromium levels to current environmental  
9 regulations. Despite the remarkable Cr(VI) removal efficiency achieved by N25 particles,  
10 passivation of the nZVI surface showed to limit the removal capacity of the material. This  
11 effect is produced by an outer layer containing Fe(III) - Cr(III) mixed oxides/oxyhydroxides  
12 that prevents penetration of the pollutant and stops the electron transfer from inner Fe<sup>0</sup> to  
13 Cr(VI) in the aqueous phase. Raman and XPS analysis, combined with sputtering experiments  
14 shed light over the composition of the external layer, which, before treatment is exclusively  
15 composed of mixed iron oxides (mainly magnetite); after the treatment, a structure of  
16 hydroxchromites  $\rightarrow$  magnetite  $\rightarrow$  Fe<sup>0</sup> is developed towards the core of the nZVI, together  
17 with a decreasing Fe(II) gradient.

#### 18 19 **Supplementary Data**

20 Experimental setup, characterization of N25 Fresh by XRD, Raman and SEM, XPS  
21 and additional fitting methodology are provided in the SD.

22

## 1 Acknowledgements

2 This work was supported by Agencia Nacional de Promoción Científica y Tecnológica  
3 (ANPCyT, Argentina) PICT projects 512-2006 and 0463-2011. A special mention to Eng. Jan  
4 Slunský from NANO IRON, s.r.o. Contributions by Martha Ortiz to the TXRF measurements  
5 and Adriana Domínguez for SEM images are gratefully acknowledged.

## 7 References

- 8 [1] B. Saha, C. Orvig, Biosorbents for hexavalent chromium elimination from industrial and  
9 municipal effluents, *Coordin. Chem. Rev.*, 254 (2010) 2959–2972.
- 10 [2] WHO, Guidelines for drinking-water quality, fourth ed., World Health Organization,  
11 Geneva, 2011.
- 12 [3] A. Baral, R.D. Engelken, Chromium-based regulations and greening in metal finishing  
13 industries in the USA, *Environ. Sci. Policy*, 5 (2002) 121–133.
- 14 [4] D.W. Blowes, C.J. Ptacek, J.L. Jambor, In-Situ Remediation of Cr(VI)-Contaminated  
15 Groundwater Using Permeable Reactive Walls: Laboratory Studies, *Environ. Sci. Technol.*,  
16 31 (1997) 3348–3357.
- 17 [5] R. Rangsvivek, M.R. Jekel, Removal of dissolved metals by zero-valent iron (ZVI):  
18 Kinetics, equilibria, processes and implications for stormwater runoff treatment, *Water Res.*,  
19 39 (2005) 4153–4163.
- 20 [6] M. Gheju, A. Iovi, Kinetics of hexavalent chromium reduction by scrap iron, *J. Hazard.*  
21 *Mater.*, 135 (2006) 66–73.
- 22 [7] M.A. Hashim, S. Mukhopadhyay, J.N. Sahu, B. Sengupta, Remediation technologies for  
23 heavy metal contaminated groundwater, *J. Environ. Manage.*, 92 (2011) 2355–2388.
- 24 [8] Y. Mamindy-Pajany, C. Hurel, F. Geret, M. Roméo, N. Marmier, Comparison of mineral-  
25 based amendments for ex-situ stabilization of trace elements (As, Cd, Cu, Mo, Ni, Zn) in  
26 marine dredged sediments: A pilot-scale experiment, *J. Hazard. Mater.*, 252-253 (2013) 213-  
27 219.
- 28 [9] M. Gheju, I. Balcu, Removal of chromium from Cr(VI) polluted wastewaters by reduction  
29 with scrap iron and subsequent precipitation of resulted cations, *J. Hazard. Mater.*, 196 (2011)  
30 131-138.
- 31 [10] W.X. Zhang, Nanoscale iron particles for environmental remediation: An overview, *J.*  
32 *Nanopart. Res.*, 5 (2003) 323–332.
- 33 [11] X.-q. Li, W.-x. Zhang, Sequestration of Metal Cations with Zerovalent Iron  
34 Nanoparticles A Study with High Resolution X-ray Photoelectron Spectroscopy (HR-XPS), *J.*  
35 *Phys. Chem. C*, 111 (2007) 6939–6946.

- 1 [12] T. Pradeep, Anshup, Noble metal nanoparticles for water purification: A critical review,  
2 Thin Solid Films, 517 (2009) 6441-6478.
- 3 [13] M.E. Morgada, I.K. Levy, V. Salomone, S.S. Farías, G. López, M.I. Litter, Arsenic (V)  
4 removal with nanoparticulate zerovalent iron: Effect of UV light and humic acids, Catal.  
5 Today, 143 (2009) 261-268.
- 6 [14] W. Yan, A.A. Herzing, C.J. Kiely, W.-x. Zhang, Nanoscale zero-valent iron (nZVI):  
7 Aspects of the core-shell structure and reactions with inorganic species in water, J. Contam.  
8 Hydrol, 118 (2010) 96-104.
- 9 [15] R.A. Crane, T.B. Scott, Nanoscale zero-valent iron: Future prospects for an emerging  
10 water treatment technology, J. Hazard. Mater., 211-212 (2012) 112-125.
- 11 [16] Y. Wu, J. Zhang, Y. Tong, X. Xu, Chromium (VI) reduction in aqueous solutions by  
12 Fe<sub>3</sub>O<sub>4</sub>-stabilized Fe<sup>0</sup> nanoparticles, J. Hazard. Mater., 172 (2009) 1640-1645.
- 13 [17] T.B. Scott, I.C. Popescu, R.A. Crane, C. Noubactep, Nano-scale metallic iron for the  
14 treatment of solutions containing multiple inorganic contaminants, J. Hazard. Mater., 186  
15 (2011) 280-287.
- 16 [18] R.M. Powell, R.W. Puls, S.K. Hightower, D.A. Sabatini, Coupled Iron Corrosion and  
17 Chromate Reduction: Mechanisms for Subsurface Remediation, Environ. Sci. Technol., 29  
18 (1995) 1913-1922.
- 19 [19] R.W. Puls, D.W. Blowes, R.W. Gillham, Long-term performance monitoring for a  
20 permeable reactive barrier at the U.S. Coast Guard Support Center, Elizabeth City, North  
21 Carolina, J. Hazard. Mater., 68 (1999) 109-124.
- 22 [20] T. Lee, H. Lim, Y. Lee, J.W. Park, Use of waste iron metal for removal of Cr(VI) from  
23 water, Chemosphere, 53 (2003) 479-485.
- 24 [21] J. Cao, W.X. Zhang, Stabilization of chromium ore processing residue (COPR) with  
25 nanoscale iron particles, J. Hazard. Mater., 132 (2006) 213-219.
- 26 [22] M. Gheju, Hexavalent Chromium Reduction with Zero-Valent Iron (ZVI) in Aquatic  
27 Systems, Water Air Soil Poll., 222 (2011) 103-148.
- 28 [23] B.A. Manning, J.R. Kiser, H. Kwon, S.R. Kanel, Spectroscopic investigation of Cr(III)-  
29 and Cr(VI)-treated nanoscale zerovalent iron, Environ. Sci. Technol., 41 (2006) 586-592.
- 30 [24] X.-q. Li, J. Cao, W.-x. Zhang, Stoichiometry of Cr(VI) immobilization using nanoscale  
31 zerovalent iron (nZVI): A study with high-resolution X-ray photoelectron spectroscopy (HR-  
32 XPS), Ind. Eng. Chem. Res., 47 (2008) 2131-2139.
- 33 [25] Z. Ai, Y. Cheng, L. Zhang, J. Qiu, Efficient removal of Cr(VI) from aqueous solution  
34 with Fe@Fe<sub>2</sub>O<sub>3</sub> core-shell nanowires, Environ. Sci. Technol., 42 (2008) 6955-6960.
- 35 [26] Q. Wang, N. Cissoko, M. Zhou, X. Xu, Effects and mechanism of humic acid on  
36 chromium(VI) removal by zero-valent iron (Fe<sup>0</sup>) nanoparticles, Phys. Chem. Earth, 36 (2011)  
37 442-446.
- 38 [27] L. Alidokht, A.R. Khataee, A. Reyhanitabar, S. Oustan, Reductive removal of Cr(VI) by  
39 starch-stabilized Fe<sup>0</sup> nanoparticles in aqueous solution, Desalination, 270 (2011) 105-110.
- 40 [28] J.-H. Kim, J.-H. Kim, V. Bokare, E.-J. Kim, Y.-Y. Chang, Y.-S. Chang, Enhanced  
41 removal of chromate from aqueous solution by sequential adsorption-reduction on  
42 mesoporous iron-iron oxide nanocomposites, J. Nanopart. Res., 14 (2012) 1-12.

- 1 [29] X. Lv, Y. Hu, J. Tang, T. Sheng, G. Jiang, X. Xu, Effects of co-existing ions and natural  
2 organic matter on removal of chromium (VI) from aqueous solution by nanoscale zero valent  
3 iron (nZVI)-Fe<sub>3</sub>O<sub>4</sub> nanocomposites, *Chem. Eng. J.*, 218 (2013) 55-64.
- 4 [30] C. Noubactep, A critical review on the process of contaminant removal in Fe<sup>0</sup>-H<sub>2</sub>O  
5 systems, *Environ. Technol.*, 29 (2008) 909-920.
- 6 [31] B.A. Balko, P.G. Tratnyek, Photoeffects on the reduction of carbon tetrachloride by zero-  
7 valent iron, *J. Phys. Chem. B*, 102 (1998) 1459-1465.
- 8 [32] M.M. Scherer, B.A. Balko, P.G. Tratnyek, The role of oxides in reduction reactions at  
9 the metal-water interface, in: *ACS Symposium Series*, 1998, pp. 301-322.
- 10 [33] C. Noubactep, A. Schöner, P. Woaf, Metallic iron filters for universal access to safe  
11 drinking water, *Clean - Soil, Air, Water*, 37 (2009) 930-937.
- 12 [34] ASTM, Standards D 1687-92, (1999).
- 13 [35] E.B. Sandell, Colorimetric determination of trace metals, in, Interscience Publishers Inc.,  
14 New York, 1959, pp. 537-542.
- 15 [36] G. Custo, M.I. Litter, D. Rodríguez, C. Vázquez, Total reflection X-ray fluorescence  
16 trace mercury determination by trapping complexation: Application in advanced oxidation  
17 technologies, *Spectrochimica Acta Part B: Atomic Spectroscopy*, 61 (2006) 1119-1123.
- 18 [37] Z. Fang, X. Qiu, R. Huang, X. Qiu, M. Li, Removal of chromium in electroplating  
19 wastewater by nanoscale zero-valent metal with synergistic effect of reduction and  
20 immobilization, *Desalination*, 280 (2011) 224-231.
- 21 [38] X. Lv, J. Xu, G. Jiang, J. Tang, X. Xu, Highly active nanoscale zero-valent iron (nZVI)-  
22 Fe<sub>3</sub>O<sub>4</sub> nanocomposites for the removal of chromium(VI) from aqueous solutions, *Journal of*  
23 *Colloid and Interface Science*, 369 (2012) 460-469.
- 24 [39] F. dos Santos Coelho, J.D. Ardisson, F.C.C. Moura, R.M. Lago, E. Murad, J.D. Fabris,  
25 Potential application of highly reactive Fe(0)/Fe<sub>3</sub>O<sub>4</sub> composites for the reduction of Cr(VI)  
26 environmental contaminants, *Chemosphere*, 71 (2008) 90-96.
- 27 [40] A.F. White, M.L. Peterson, Reduction of aqueous transition metal species on the surfaces  
28 of Fe(II)-containing oxides, *Geochimica et Cosmochimica Acta*, 60 (1996) 3799-3814.
- 29 [41] N. Melitas, O. Chuffe-Moscoso, J. Farrell, Kinetics of Soluble Chromium Removal from  
30 Contaminated Water by Zerovalent Iron Media: Corrosion Inhibition and Passive Oxide  
31 Effects, *Environ. Sci. Technol.*, 35 (2001) 3948-3953.
- 32 [42] R.M. Cornell, U. Schwertmann, Products of Iron Metal Corrosion, in: *The Iron Oxides*,  
33 Wiley-VCH Verlag GmbH & Co. KGaA, Darmstadt, 2004, pp. 491-508.
- 34 [43] Moulder J., Stickle W., Sobol P., B. K., *Handbook of X-ray Photoelectron Spectroscopy*,  
35 Eden Prairie, Minnesota, 1992.

36

37

1 Table 1

2 Mass of Cr(VI) removed per gram of nZVI for different nZVI materials.

mg Cr(VI)/g nZVI	pH	Reference
10.06	6.36	Ai et al. 2008 [25]
50 - 180	4 - 8	Li et al. 2008 [24]
34.1	6	Kim et al. 2012 [28]
62.4	6	Wang et al.2011 [26]
20.16	5	Alidokht et al. 2011 [27]
180	4.82	Fang et al. 2011 [37]
100	3	Lv et al. 2012 [38]
47.2 ± 0.1	5	This work
411 ± 24	3	This work

3

4

5

1     **Highlights**

2

- 3     1. An outstanding Cr(VI) removal was achieved with these nZVI in only 30 minutes.  
4     2. The passive outer layer formed after treatment prevents further Cr(VI) removal.  
5     3. Cr(III) is the only chromium species at the external layer after reaction.  
6     4. A structure of hydroxchromites → magnetite → Fe<sup>0</sup> developed towards the core of  
7     the nZVI.  
8

9

ACCEPTED MANUSCRIPT